

The Dynamics of Neptune Trojan: I. the Inclined Orbits

Li-Yong Zhou^{1*}, Rudolf Dvorak², Yi-Sui Sun¹

¹*Department of Astronomy, Nanjing University, Nanjing 210093, China*

²*Institute for Astronomy, University of Vienna, Türkenschanzstr. 17, A-1180 Wien, Austria*

Accepted . Received

ABSTRACT

The stability of Trojan type orbits around Neptune is studied. As the first part of our investigation, we present in this paper a global view of the stability of Trojans on inclined orbits. Using the frequency analysis method based on the FFT technique, we construct high resolution dynamical maps on the plane of initial semimajor axis a_0 versus inclination i_0 . These maps show three most stable regions, with i_0 in the range of $(0^\circ, 12^\circ)$, $(22^\circ, 36^\circ)$ and $(51^\circ, 59^\circ)$ respectively, where the Trojans are most probably expected to be found. The similarity between the maps for the leading and trailing triangular Lagrange points L_4 and L_5 confirms the dynamical symmetry between these two points. By computing the power spectrum and the proper frequencies of the Trojan motion, we figure out the mechanisms that trigger chaos in the motion. The Kozai resonance found at high inclination varies the eccentricity and inclination of orbits, while the ν_8 secular resonance around $i_0 \sim 44^\circ$ pumps up the eccentricity. Both mechanisms lead to eccentric orbits and encounters with Uranus that introduce strong perturbation and drive the objects away from the Trojan like orbits. This explains the clearance of Trojan at high inclination ($> 60^\circ$) and an unstable gap around 44° on the dynamical map. An empirical theory is derived from the numerical results, with which the main secular resonances are located on the initial plane of (a_0, i_0) . The fine structures in the dynamical maps can be explained by these secular resonances.

Key words: Planets and satellites: individual: Neptune – Minor planets, asteroids – Celestial mechanics – Method: miscellaneous

1 INTRODUCTION

In the restricted three-body model consisting of the Sun, a planet and an asteroid, the equilateral triangular Lagrange equilibrium points (L_4 and L_5) are stable for all planets in our Solar system. Asteroids in the vicinities of L_4 and L_5 of a parent planet are called Trojans after the group of asteroids found around Jupiter’s Lagrange points. Objects on Trojan like orbits around Mars and (temporarily) around Earth have been observed while the Trojan-type orbits of Saturn and Uranus have been proven unstable due to the perturbations from other planets.

As for Neptune, the possibility of stable orbits around the Lagrange points have been verified in several papers, e.g. (Holman & Wisdom 1993; Weissman & Levison 1997; Nesvorný & Dones 2002), before the discovery of the first Neptune Trojan, 2001 QR322 (Pittichova et al. 2003). Up to now, 6 Neptune Trojans have been discovered¹ around Neptune’s L_4 point. We list their orbital properties in

Table 1. It is suspected that there could be much more Trojan-type asteroids sharing the orbit with Neptune than with Jupiter, both in the sense of number and total mass (Sheppard & Trujillo 2006). After these discoveries, more papers were devoted to the issue of Neptune Trojans, focusing either on the orbital stability and origin of specific objects (Brasser et al. 2004b; Li, Zhou & Sun 2007) or on creating a global view of stable regions around the Lagrange points, e.g. (Marzari, Tricarico & Scholl 2003a; Dvorak et al. 2007; Dvorak, Lhotka & Schwarz 2008). Both the observing and the theoretical studies of Neptune Trojans could give important clues on how these objects were trapped into their current orbits, where and when the planet Neptune formed and how the orbits of the outer planets evolved in the early stage of the formation of the Solar system. Therefore, it is worth to investigate the orbital stability of fictitious Trojans in the whole parameter space.

All the Trojans in Table 1 are on near-circular orbits (with quite small value of eccentricity) and two of them have high inclination values. The stability and origin of inclined orbit is an interesting topic (Li, Zhou & Sun 2007). As the first part of our investigation of the whole phase space, we study in this paper the orbital stability of Trojans on in-

* zhouly@nju.edu.cn

¹ IAU: Minor Planet Center, <http://www.cfa.harvard.edu/iau/lists/NeptuneTrojans.html>

Table 1. Orbits of 6 observed Neptune Trojans, given at epoch JD=2454800.5 with respect to the mean ecliptic and equinox at J2000.0. The perihelion argument ω , ascending node Ω and inclination i are in degrees.

Designation	M	ω	Ω	i	e	a (AU)
2001 QR322	57.88	160.8	151.6	1.3	0.031	30.302
2004 UP10	341.28	358.5	34.8	1.4	0.028	30.212
2005 TN53	287.04	85.7	9.3	25.0	0.065	30.179
2005 TO74	268.10	302.6	169.4	5.3	0.052	30.190
2006 RJ103	238.64	27.1	120.8	8.2	0.028	30.077
2007 VL305	352.88	215.2	188.6	28.1	0.064	30.045

clined orbits and try to find out the possible regions where the potential primordial Trojans could survive up to present. Using the frequency analysis method, we construct dynamical maps to locate the most stable regions, and figure out the mechanisms that bring instability to the motion.

Since the L_5 point of Neptune is nowadays in the direction of the Galaxy center thus not suitable for asteroid observing, it is not astonishing to see all asteroids listed in Table 1 are around the L_4 point. Observations show that there are more objects around Jupiter's L_4 than the L_5 point, and such an asymmetry between L_4 and L_5 was also reported for Neptune (Holman & Wisdom 1993). The origin of this asymmetry is discussed too in this paper.

This paper is organized as follows. In Section 2, we introduce the dynamical model and the spectral analysis method applied in our study. We also show that the apparent asymmetry between L_4 and L_5 is only an artificial effect from the asymmetrical selection of initial conditions. Section 3 presents the dynamical maps around the L_4 and L_5 points. We describe the structures seen in the maps, and show that the Kozai resonance and the ν_8 secular resonance are primarily responsible for the interesting features of the maps. In Section 4, the dynamical spectra of motion are constructed and a semi-analytical theory of secular resonance is derived. Finally, the conclusions are given in Section 5.

2 MODEL AND METHOD

2.1 Dynamical model

We numerically simulated the orbital evolution of thousands of test particles around the Lagrange points of Neptune and investigated their orbital stability with a method based on the spectral analysis on the outcome of numerical integrations. Our dynamical model includes the Sun (with the inner planets masses added onto), four outer planets (Jupiter, Saturn, Uranus and Neptune) and the Trojans. The Sun and planets gravitationally interact among themselves and on the Trojans, but each Trojan is assumed massless and therefore has no effect on other bodies.

Since the Lagrange points are defined in the restricted three-body problem, we set the initial orbital elements of the fictitious Trojans referring to Neptune's orbit. A Trojan-like asteroid shares the same orbit with the planet and they are in fact in a 1:1 mean motion resonance. For Neptune's Trojan, the critical argument of this resonance is

$$\sigma = \lambda - \lambda_8 \quad (1)$$

where $\lambda = \omega + \Omega + M$ is the mean longitude and the subscript '8' denotes Neptune (hereafter the orbital elements of planets are subscripted with '5, 6, 7' and '8' for Jupiter, Saturn, Uranus and Neptune as usual). We initially set $\sigma_0 = \sigma_c$ where σ_c is the center of the tadpole orbits. This center is near $\pm 60^\circ$ for near-circular and coplanar orbit and varies with the semimajor axis, eccentricity and inclination of the Trojan. Since σ_c changes slightly with a and i (Namouni 1999; Nesvorný et al. 2002), we may still set $\sigma_c = \pm 60^\circ$ approximately.

Referring to the previous analysis (Nesvorný & Dones 2002; Nesvorný et al. 2002) and to ensure a coverage of the representative region around the Lagrange points, the choice of the initial angular variables for the fictitious Trojans is made as below. The argument of perihelion ω_0 is set as $\omega_0 - \omega_8 = 60^\circ$ for L_4 (-60° for L_5), while the ascending node Ω_0 and the mean longitude M_0 are the same as that of Neptune $\Omega_0 = \Omega_8, M_0 = M_8$. After some test simulations, the initial semimajor axes a_0 of the test particles are determined to be evenly sampled in the range from 29.72 AU to 30.32 AU for L_4 and from 29.90 AU to 30.50 AU for L_5 . Note these two ranges of a are different from each other (see a discussion in the following section).

The observed Neptune Trojans all have small eccentricities but their inclinations are widely spread, particularly, two of them have high inclinations 25° and 28° . In this paper, we focus on the dynamics of inclined orbits, and therefore we fix the initial eccentricity of test particles at $e_0 = e_8 = 0.00625 \approx 0$ (nearly circular) and vary the initial inclination i_0 from 0° to 70° with an increment of 1.25° .

In the above arrangement, the initial value of the resonant argument σ is always at the libration center. For a Trojan, the argument σ generally librates around the center σ_c with a nonzero amplitude D , and simultaneously the semimajor axis a oscillates with an amplitude d around a mean value given by the semimajor axis of Neptune. It has been shown (Érdi 1988; Milani 1993) that the values of d and D are constant in the simplest approximation and they are related to each other by:

$$\frac{d}{D} = \sqrt{3\mu a_8} + \dots \approx 0.373, \quad (2)$$

where μ is the mass of Neptune measured in the solar mass, d is measured in AU and D in radians. For this reason, having different a_0 values, we do not need to test different initial value of σ .

Given the proper initial conditions, the systems are then integrated with a Lie-integrator (Hanslmeier & Dvorak 1984). In some cases, we use also the *hybrid symplectic integrator* in the Mercury6 software package (Chambers 1999) to compare the results and to simulate the orbital evolution for the lifespan of the solar system (4.5 Gyr).

2.2 Spectral analysis

During the integration of the system, the orbits of the fictitious Trojans are recorded for further analyzing. The Lie-integrator outputs the orbits at every equal time interval so that we can apply a Fast Fourier Transform (FFT) method to the orbital variables. The power spectra of these variables then can be used to give information about the dynamical behavior of the orbits. On one hand, the system must be

integrated to a time long enough to reveal the secular behavior; on the other hand, if we record the orbits in such a long time span, the data to be analyzed would be by far too large.

The amount of the output data can be reduced by increasing the time interval at which the output is recorded. But the risk of losing valuable information and/or introducing artificial features arises from the large sampling period. As a compromise, a low-pass digital filter is introduced to remove the short-period terms, which generally are not crucial and can be cut off by the average procedure (Carpino, Milani & Nobili 1987). Then we collect the records from the filtered output at every tens-of-times sampling intervals thus the amount of data is largely reduced. A digital filter supplied by T. Michtchenko is applied in this paper. See (Michtchenko & Ferraz-Mello 1995; Michtchenko et al. 2002), where the details about this filter and its application can be found.

After some test runs, we carefully choose an output interval of 4 yr. The output data are then smoothed through the filtering process and among the filtered data a sampling interval of $\Delta = 512$ yr is adopted. This interval is shorter than all the secular periods in the outer solar system, such that all information on the long-term effects is preserved. Finally, the systems are integrated to $\sim 3.4 \times 10^7$ yr and totally $N = 65,536 (= 2^{16})$ lines of the filtered orbital variables including a, e, i, σ etc are recorded for further analyzing. The sampling interval determines the Nyquist frequency $f_{\text{Nyq}} = \frac{1}{2\Delta} = 9.766 \times 10^{-4} \text{ yr}^{-1}$, while the frequency resolution calculated from this data through an FFT is $f_{\text{res}} = \frac{1}{N\Delta} = 2.980 \times 10^{-8} \text{ yr}^{-1}$. We have tried smaller output intervals that can cover short period effects such as the quasi 5:2 mean motion resonance between Jupiter and Saturn (the Great Inequality, with a period of ~ 880 yr) but did not find any crucial effects with periods shorter than 10^3 yr in the motion of Neptune Trojans.

An FFT to the output data provides us valuable information about the orbital dynamics, and it allows us to determine the regularity of an orbit. Generally, a regular orbit is characterized by quasi-periodic terms, so that the power spectra of the orbital elements of this orbit are dominated by a countable (small) number of frequency components. On the contrary, a chaotic orbit is not quasi-periodic and the independent frequencies of the motion change with time, such that the power spectrum consists of broadband components and is characterized by strong noise. To tell the difference between the spectra of regular and chaotic motion, we can count the spectral peaks above a given noise level, and the number obtained is defined as the *spectral number* (SN hereafter). Obviously, a small SN indicates a regular motion while a large one implies a chaotic motion. The SN has been successfully applied to indicate the regularity of the main-belt asteroids (Michtchenko & Ferraz-Mello 1995; Michtchenko et al. 2002) and extra solar planets (Ferraz-Mello et al. 2005; Michtchenko, Beaugé & Ferraz-Mello 2008). We use this indicator to construct the *dynamical map* in Section 3.

2.3 L_4 versus L_5

Since long ago, the asymmetrical distribution of stable regions around Neptune's L_4 and L_5 points puzzles. For exam-

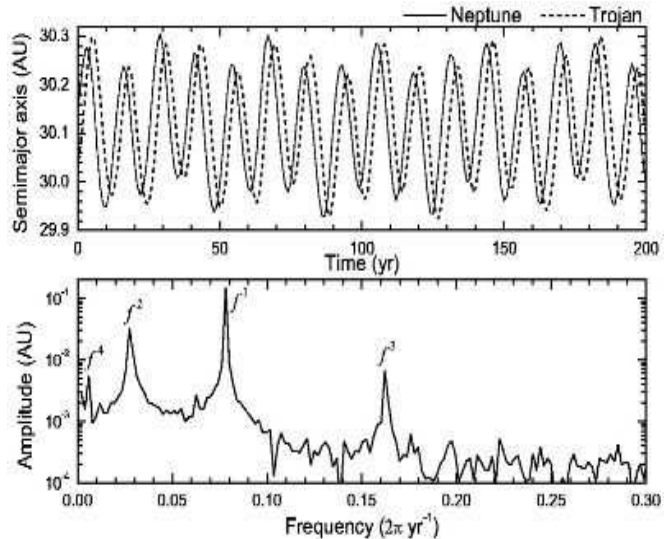


Figure 1. Upper panel: The temporal variation of the osculating semimajor axes of Neptune and of the Trojan at the resonance center. Lower panel: the power spectrum of the Trojan's semimajor axis in the above panel.

ple, a shift in the semimajor axis of stable regions around L_4 and L_5 was found when test particles in the outer solar system were integrated to 20 Myr (Holman & Wisdom 1993). Nesvorný and Dones Nesvorný & Dones (2002) argued that the asymmetrical distributions of stable region was nothing more than an artificial effects rising from selections of initial conditions. When we set the initial conditions for test particles referring to the osculating orbit of Neptune, generally they are symmetrically distributed around the L_4 and L_5 points. It is worth emphasizing that this symmetry is only valid in the frame consisting of the Sun, Neptune and the asteroid. But the real system evolves symmetrically with respect to the barycenter, which is not exactly in the Sun. In this sense, the initial conditions around L_4 and L_5 are not symmetric to each other any longer. Such an argument was also proposed by Marzari et al. Marzari, Tricarico & Scholl (2003a). More recently, Dvorak et al. Dvorak, Lhotka & Schwarz (2008) showed by sophisticated numerical experiments that a proper selection of initial conditions can remove the difference between L_4 and L_5 . Nevertheless, we would like to show here another evidence: we construct separately two dynamical maps for Trojans around the L_4 and L_5 (see Figs. 2 and 3). Judging from the appearances, they are symmetrical to each other, only except a shift in the semimajor axis, which we analyze below.

Given the initial orbital elements of 101 test Trojans as $e_0 = e_8, i_0 = i_8, \omega_0 = \omega_8 + 60^\circ, \Omega_0 = \Omega_8, M_0 = M_8$ and a_0 varying from 29.9 AU to 30.5 AU, we integrate the system up to 3.4×10^4 yr (the typical libration period of σ is $\sim 9 \times 10^3$ yr, see Chap. 3.8 of (Murray & Dermott 1999)) and calculate the amplitude $\Delta\sigma$ of the librating resonant argument σ for each Trojan. The value of a_0 at which $\Delta\sigma$ meets the minimum, assigned a_0^{min} , is regarded as the center of the tadpole orbits around L_4 point. At a specific moment t , the osculating orbits of planets lead to one value of $a_0^{\text{min}}(t)$. At next moment t' , the planets have evolved to new osculating orbits. We restart the above-mentioned calculations with planets on the new osculating orbits, but the fictitious

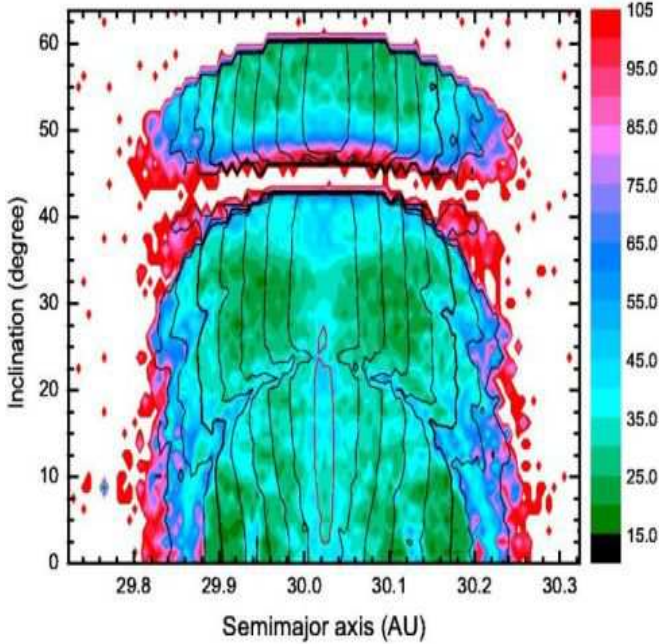


Figure 2. The dynamical map around L_4 point. The color indicates the spectral number. Green indicates regular motion, while red is on the edge of chaotic motion. From our experiences (see Section 3.2), those orbits with $SN > 50$ are roughly not to be expected to survive in the lifespan of the solar system. The libration amplitude $\Delta\sigma$ of the resonant angle is also mapped by contour curves. Among them, the red contour curve represents $\Delta\sigma = 10^\circ$ while the thick black one is for $\Delta\sigma = 60^\circ$.

Trojans still on the same initial orbits as before. A new value of the central semimajor axis $a_0^{\min}(t')$ is obtained. In such a way, we finally get two series of semimajor axes, one is for Neptune’s oscillating orbit and the other for the corresponding Trojan at the resonance center. We show the time variations of them in Fig. 1.

Applying an FFT to the time series of the central a_0^{\min} in the upper panel, we get the power spectrum in the lower panel of Fig. 1. The frequencies of the peaks tell us the mechanism causing the variation of a_0^{\min} . The highest four peaks are at $f^1 = 0.0781$, $f^2 = 0.0273$, $f^3 = 0.162$ and $f^4 = 0.00549$ ($2\pi/\text{yr}$). Denoting the mean motion (orbital frequency) of planets by f_5, f_6, f_7 and f_8 , a simple calculation reveals that $f^1 = f_5 - f_8$, $f^2 = f_6 - f_8$, $f^3 = 2f_5$ and $f^4 = f_7 - f_8$, that is, these frequencies are either the synodic frequencies ($f^{1,2,4}$) or the harmonics (f^3) of orbital frequencies in the outer solar system. This fact demonstrates again that the asymmetrical “shift” in the semimajor axis of the center of the tadpole orbits is only due to the initial orbital configurations of planets. Because of its largest mass, Jupiter plays the most distinct role in causing this variation.

3 RESULTS

3.1 Dynamical map

We present our investigations on the dynamics of the inclined Trojans in this part. As mentioned above, the value of the libration center σ_c changes only slightly with inclination, and therefore we may fix its value at 60° for L_4 and

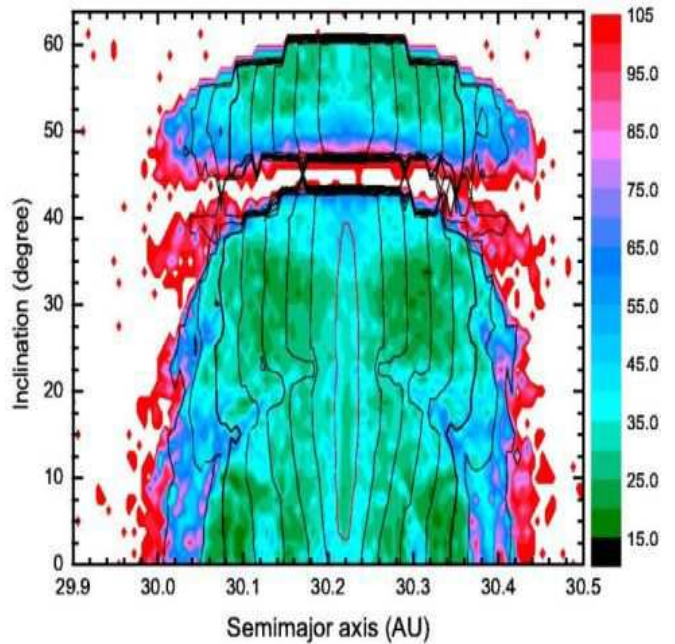


Figure 3. The same as Fig. 2 but for L_5 point.

-60° for L_5 when we study the dependence of stability on the orbital inclination.

Adopting the spectral number as an indicator of the regularity of orbits, we construct dynamical maps using 5757 orbits starting from a 101×57 grid on the (a_0, i_0) plane and integrated for 34 Myr. The power spectrum of $\cos \sigma$ for each orbit is calculated and the number of peaks, which are over one percent of the highest peak, is defined as the SN. To limit the number into a manageable range, an SN is forced to be 100 if it was originally larger than that. We also exclude orbits that escape from the 1:1 resonance region. A simple criterion is applied: if the averaged value of the semimajor axis a of a test particle does not satisfy $29.9 \text{ AU} < \bar{a} < 30.5 \text{ AU}$, it is regarded as escaped from the resonance, and an SN of 110 is assigned to the orbit. We show the dynamical maps in Fig. 2 for L_4 and in Fig. 3 for L_5 . Because all orbits with inclination higher than 61° can not survive in the Trojan-like orbit, we show in Figs. 2 and 3 only for orbits with $i_0 \in [0^\circ, 63.75^\circ]$.

The colour in the dynamical map indicates the SN. In the green region where SN is relatively small, the motion is dominated by a few dominating frequencies and thus it is more regular; but in the blue and red region, the spectrum of $\cos \sigma$ is characterized by strong noise and thus the motion is chaotic; the white color with $SN = 110$ indicates escaped orbits.

The dynamical maps in Figs. 2 and 3 do not show any asymmetry between L_4 and L_5 . The only distinguishable difference between them is a shift in the semimajor axis, which is due to the setting of initial conditions, as described in Section 2. Hereafter in this paper, we will discuss only the Trojans around the L_5 point (Fig. 3). We believe that the results can be mirrored to the L_4 point.

Judging from the dynamical maps, the most regular orbits mainly exist in three regions in inclination: A: $0^\circ - 12^\circ$, B: $22^\circ - 36^\circ$, and C: $51^\circ - 59^\circ$, approximately. The region

A and B are connected by a less regular region, but region C is apparently separated from others by an unstable gap at $i_0 \sim 44^\circ$. Note the inclination values of the observed Trojans in Table 1 in fact reside in region A and B. Except for the white-colored region, our results do not repel the possibility of Trojans outside regions A, B and C, but we argue that the probability of finding Trojans there is lower. Particularly, region C at high inclination is isolated from regions A and B, therefore any Trojans found in region C should have been always there, i.e. they must be primordial. The upper limit of region C is consistent with the value (61.5°) given in a restricted three-body model (Brasser, Heggie & Mikkola 2004a). The upper limit of region B is very close to the value (35°) given in (Nesvorný & Dones 2002), where the authors argued that no Trojan with higher inclination could survive. By plotting “diffusion maps” for initial inclination i_0 at $0^\circ, 10^\circ, 20^\circ$ and 30° , Marzari et al. Marzari, Tricarico & Scholl (2003a) found two “high stability regions” locating respectively at $i_0 = 0^\circ$ and $i_0 = 30^\circ$. They have used the slice of phase space at definite inclinations, and the two stable slices reported by them are well inside region A and region B.

The coplanar orbits are not necessarily more regular than the inclined ones. In fact, there are two less regular “holes” at low inclination $i_0 < 5^\circ$ and around $a_0 \sim 30.13, 30.31$ AU in Fig. 3. The central area, in which the libration amplitude is small, is likewise not necessarily more safe for Trojans. Different secular resonances are crowded in this area and their overlappings may introduce chaos.

We also calculated the libration amplitude of the resonant argument σ . Here by “amplitude” we mean the difference between the maximum and minimum values of σ during our integration time, $\Delta\sigma = \sigma_{\max} - \sigma_{\min}$. The contour of $\Delta\sigma$ is also plotted in Figs. 2 and 3. It has been shown in previous literatures (Weissman & Levison 1997; Nesvorný & Dones 2002) that $\Delta\sigma$ should not exceed $60^\circ - 70^\circ$ for stable orbits in the resonance. In fact the green (regular) region in Figs. 2, 3 is shaped by the contour curve of $\Delta\sigma = 60^\circ$. But for small inclination $i_0 < 10^\circ$ there are some regular orbits having $\Delta\sigma \sim 70^\circ$. The most regular orbits in region A, B and C have libration amplitude of $20^\circ - 60^\circ$. Submit $\Delta\sigma = 60^\circ$ ($D = \pi/3$) into Eq.(2), we get the oscillating amplitudes of semimajor axis $d \approx 0.39$ AU. It is a little larger than the value obtained from Fig. 3 (~ 0.31 AU), which is shrunk by perturbations from other planets besides Neptune. The libration amplitude up to 60° and even to 70° indicates also that all the Trojans which survive in our integrations are on the tadpole orbits. Trojans initially on horseshoe orbits in our simulations typically escape from the resonance before 10 Myr.

The maximal eccentricity of an orbit experienced during the evolution, e_{\max} , has been used as an indicator of the chaoticity of motion (Dvorak et al. 2007; Dvorak, Lhotka & Schwarz 2008). We see from such an e_{\max} map in Fig. 4 that most of the orbits in the 1:1 mean motion resonance maintain their small eccentricity during the evolution. In those areas corresponding to green regions in Fig. 3, the eccentricity is smaller than 0.05. An interesting feature visible in Fig. 4 is a strip of relatively larger eccentricity crossing through the map at $i_0 = 11^\circ - 16^\circ$. In this strip, $e_{\max} \sim 0.05$ while in its vicinity we have $e_{\max} \sim 0.03$. There are still some other fine structures buried in the

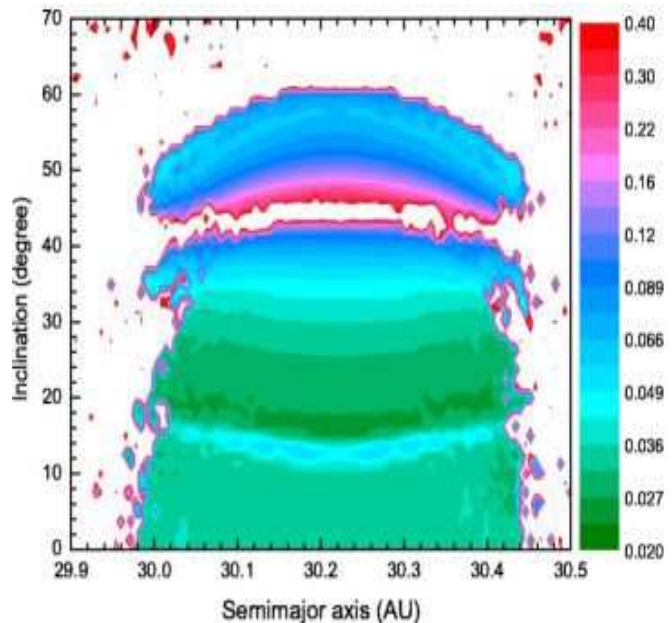


Figure 4. The maximal eccentricity e_{\max} of orbits experienced in the evolution.

dynamical map in Fig. 3 (and also, similar in Fig. 2). For example, an “arc” of less regular motion than its neighborhood, with ends at $(a_0 = 30.04 \text{ AU}, i_0 = 0^\circ)$, $(30.38 \text{ AU}, 0^\circ)$ and crossing $(30.20 \text{ AU}, 22^\circ)$, can be easily recognized in Fig. 3. This notable feature is also characterized by a constriction of the $\Delta\sigma$ contour curves, i.e. orbits initialized on this arc have larger libration amplitudes. A closer look at this region reveals that this unstable arc is encompassed exteriorly by a stable arc and an unstable but shorter arc. Another “arc structure” can be seen extending from $(a_0 = 30.02 \text{ AU}, i_0 = 20^\circ)$ to $(30.08 \text{ AU}, 30^\circ)$, which is also accompanied by a slight deformation of the $\Delta\sigma$ contours. Last but not least, both the dynamical maps in Figs. 2 and 3 are symmetric with respect to the central line $a_0 = 30.02$ AU in Fig. 2 and $a_0 = 30.20$ AU for Fig. 3), where locates the center of the tadpole orbit. This symmetry is apparent but not exact. The tiny deviation from the symmetry is well-known and has been described, e.g. in Chap. 3.9 of (Murray & Dermott 1999).

So far we have depicted the orbital stabilities of Trojans on inclined orbits with their initial eccentricities all restricted to a small value (nearly circular orbits). Certainly, the stability of a Trojan’s orbit depends on its eccentricity. In fact, the stable region in eccentricity is very limited. Nesvorný & Dones Nesvorný & Dones (2002) reported that for inclination $i = 0^\circ$ all the “low-LCE” (stable) tadpole orbits have $e < 0.1$, and they also found an orbit of $e = 0.07, i = 25^\circ$ surviving over 4 Gyr in their numerical integrations. Marzari et al. Marzari, Tricarico & Scholl (2003a) showed that in the “high stability regions” on the slices of $i_0 = 0^\circ$ and $i_0 = 30^\circ$, the proper eccentricities of Trojan orbits are small, $e_p < 0.1$ and $e_p < 0.15$ respectively.

We also calculated the dynamical maps on the (a_0, e_0) plane with specific inclination values. Our results confirm the conclusion that the eccentricities of stable orbits are restricted to small values. As examples, we show in Fig. 5 two cases with $i_0 = 5^\circ$ and $i_0 = 55^\circ$, correspondingly inside the

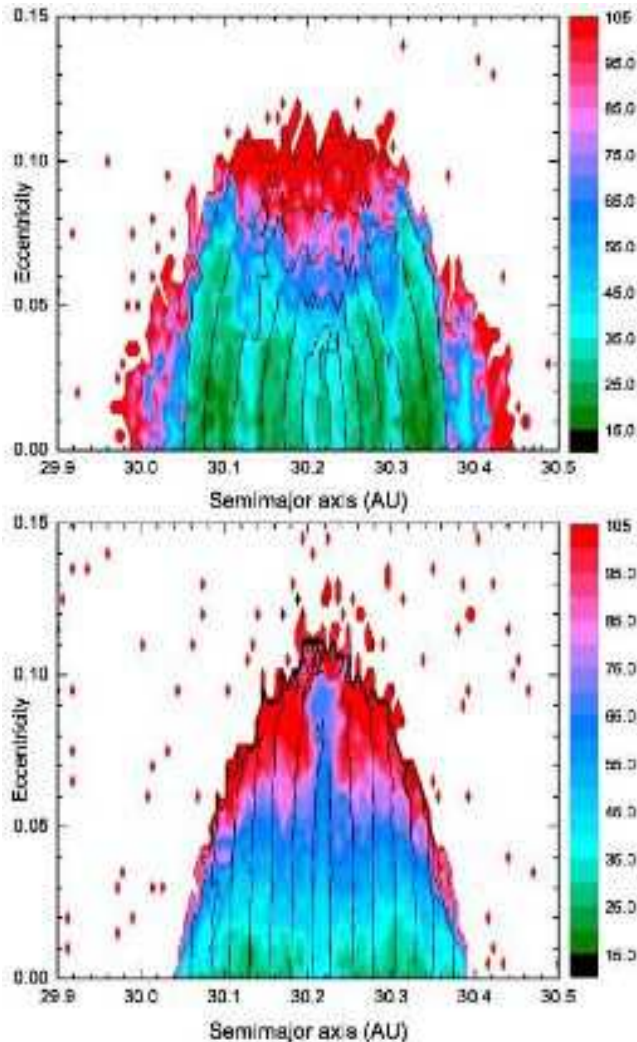


Figure 5. The dynamical maps on the (a, e) -plane for specific initial inclinations. The upper panel is for $i_0 = 5^\circ$ and the lower for $i_0 = 55^\circ$. The color codes are the same as in Fig. 2 and 3. The contour curves represent the libration amplitude of the resonant argument σ . From the inside out are contours for $\Delta\sigma = 10^\circ$ to $\Delta\sigma = 70^\circ$ with an increment of 10° .

stable region A and C. For $i_0 = 5^\circ$, an orbit with initial eccentricity as large as $e_0 \sim 0.085$ may still be among the most stable orbits and its libration amplitude may reach $\Delta\sigma \sim 70^\circ$. For $i_0 = 55^\circ$, however, the most stable region extends only below $e_0 \sim 0.02$ and the libration amplitude $\Delta\sigma < 60^\circ$. Our preliminary calculations for other slices at different inclination values show that some test particles with $e_0 \sim 0.25$ at $i_0 = 35^\circ$ may retain on the Trojan orbits in our 34 Myr integrations, but the SN indicator indicates that the eccentricity of the most stable orbit in region A, B and C, approximately, should not exceed 0.10, 0.12 and 0.03 respectively.

Only two slices have been shown here and apparently in Fig. 5 there are fine structures that bear plenty information about the orbital dynamics. Toward a global view of the stability of eccentric orbits, particularly, of the mechanisms behind, we need more slices at different inclinations and a through analysis on the orbital dynamics. This work is

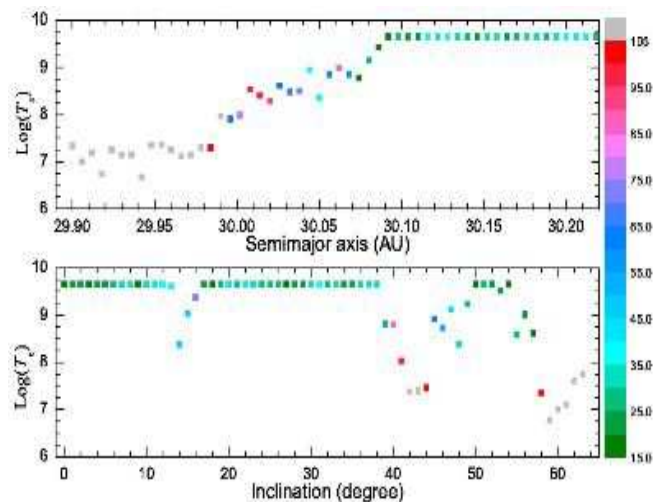


Figure 6. The lifetime (in logarithm) of orbits from the 4.5 Gyr integrations. These orbits are initialized either on the horizontal line (upper panel) or the vertical line (lower panel) on the (a_0, i_0) plane (see text for an explanation). Their spectral numbers are calculated from the short-term (3.4×10^7 yr) integration, and indicated by color. Note those orbits with SN = 110 (see text) is colored grey in this figure.

undergoing and we would like to leave this to a separated paper. From below in this paper, we will focus on the dynamics of the inclined orbits, i.e., we will analyze the mechanisms causing the structures in the dynamical maps of Figs. 2 and 3.

3.2 Spectral number and long-term stability

Before continuing to analyze the mechanisms that portrait the features of the dynamical maps, we perform some long-term orbital integrations using the Mercury6 integrator package (Chambers 1999) to compare them with the results from our Lie-integrator and to check the reliability of the indicator i.e. the spectral number.

We arbitrarily select initial Trojan orbits from two lines on the (a_0, i_0) plane. One is a horizontal line with $i_0 = 10^\circ$ and the other one is the vertical line with $a_0 = 30.098$ AU. Hundreds of orbits initialized on the lines are integrated up to the solar system age, 4.5 Gyr. An object is discarded if its semimajor axis is larger than 60 AU. A Trojan can attain such a wide orbit through close encounters with the Sun and/or planets. We do not check the time when a Trojan leaves the 1:1 resonance, but generally, an object will be scattered far away soon after it loses the protection of the 1:1 resonance.

The results are shown in Fig. 6. We note the correlation between the lifetime and the SN. Those orbits surviving the whole integration are also those with small SN while orbits with relatively larger SN escape from the resonance before the integration ends. Particularly, in the lower panel we see four orbits with $i_0 = 13^\circ, 14^\circ, 15^\circ, 16^\circ$ lose their stability after 4.2, 0.24, 1.1 and 2.4 Gyr respectively. These points are on the blue arc in Fig. 3, i.e., the chaotic property of these orbits has been correctly predicted by the relatively large SN calculated from our short-term integration.

We should point out that several orbits with small SN

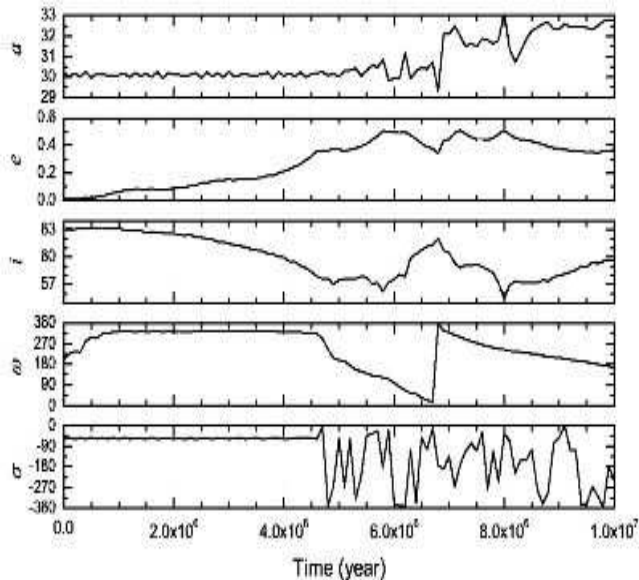


Figure 7. An example of unstable orbits ($a_0 = 30.218$ AU, $i_0 = 61.25^\circ$) trapped in the Kozai resonance. From top down, 5 panels are for semimajor axis a (in AU), eccentricity e , inclination i , argument of perihelion ω and the resonant argument σ . Angular variables are in degrees.

(green ones in Fig. 6) can not sustain the solar system age. They are all at the border of stable region, and escape only after very long evolution ($\sim 10^9$ yr). Perhaps the instability is introduced through very slow chaotic diffusion, which the SN fails to detect. Nevertheless, one can see that globally the SN is still a successful indicator of orbital stability.

Another conclusion can be made from Fig. 6, namely Trojans with high inclinations $i_0 > 50^\circ$ can survive the solar system age. $i_0 = 35^\circ$ is not the upper limit in inclination for potentially stable Trojans, as one also can see from Fig. 2 and Fig. 3.

3.3 Kozai mechanism and ν_8 resonance

The most distinguishable features in the dynamical map are two white (unstable) regions: the high inclination region with $i_0 > 61^\circ$ and an unstable gap at $i_0 \sim 44^\circ$. Orbits in these two regions are strongly chaotic and they cannot survive in the resonance even in our short-term integration. There must be some strong mechanisms driving them out.

For orbits with high inclination, the Kozai resonance (Kozai 1962; Kinoshita & Nakai 2007) is acting as the responsible mechanism. In a Kozai resonance the perihelion argument ω librates while the eccentricity and inclination undergo variations such that the quantity $H_K = \sqrt{1 - e^2} \cos i$ remains constant. When the inclination of a Trojan decreases its eccentricity increases, as a result, it will cross Uranus' orbit and the probability of close encounter with Uranus is enhanced significantly.

We checked the evolution of some orbits with $i_0 > 61^\circ$ and found that the instability is really due to the Kozai resonance. A typical orbit is shown in Fig. 7. We see clearly that ω enters a small-amplitude libration state at 0.5 Myr after a transient period. From then on ω is nearly constant,

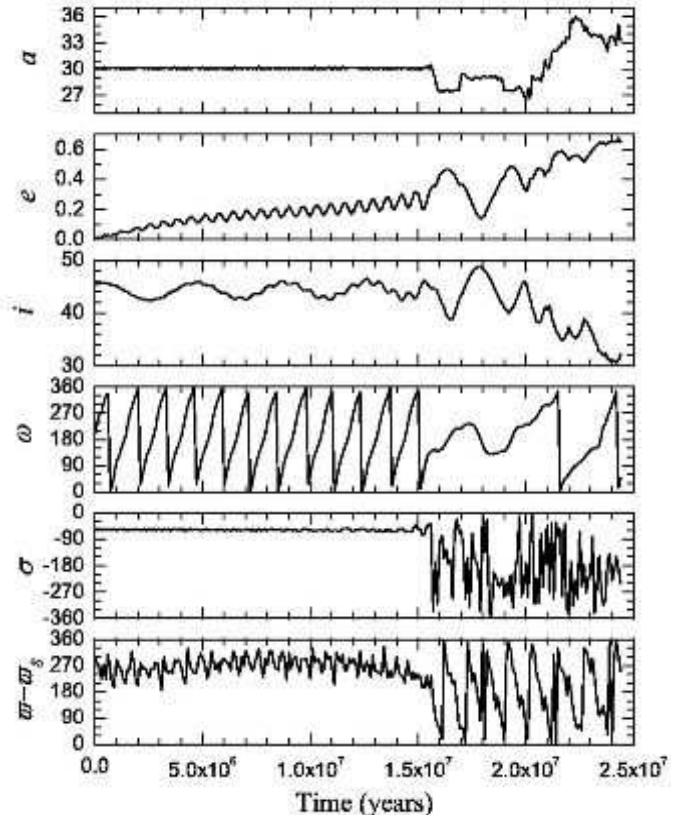


Figure 8. The evolution of a typical orbit ($a_0 = 30.218$ AU, $i_0 = 43.75^\circ$) initialized in the unstable gap. From top down, 6 panels show the temporal evolution of semimajor axis a (in AU), eccentricity e , inclination i , argument of perihelion ω , 1:1 resonant argument σ and the difference between the perihelion longitudes of the Trojan and of Neptune. All angular variables are given in degrees.

e increases as i decreases till 4.6 Myr when e reaches a value of 0.358. The perihelion distance is now $q = a(1 - e) \approx 30.20 \times (1 - 0.358) = 19.39$ AU, which is in the range of Uranus distance to the Sun. A close encounter with Uranus then destroys the 1:1 mean motion resonance between the Trojan and Neptune, as shown by the deviation of σ from libration in the bottom panel of Fig. 7. After that the object is finally scattered out from the solar system through a series of encounters with planets.

Generally, the Kozai mechanism protects an object from close encounters with the perturber (usually a planet) either for orbits at high inclination where ω librates around 90° or 270° (Thomas & Morbidelli 1996), or for orbits at low inclination where ω oscillates around 0° or 180° (Michel & Thomas 1996). But in our case of Neptune Trojans, as seen in the third panel of Fig. 7, ω librates around 322° with an amplitude smaller than 5° . To our best knowledge, there is no such an “asymmetrical” libration center of ω being reported before. However, in the case of Neptune Trojan, there are at least two facts that must be taken into account in the analysis of the Kozai resonance. First, the object is in a 1:1 mean motion resonance with Neptune, and second, there is more than one perturber on the asteroid's motion. Thus we believe the Kozai resonance here is more complicated and it deserves a careful investigation in future.

As for the unstable gap at $i_0 \sim 44^\circ$ in the dynamical map, a close look at the orbits reveals that it is due to the apsidal secular resonance ν_8 . A ν_8 secular resonance happens when the precession rate of the Trojan’s perihelion equals the fundamental frequency g_8 of the solar system, which is mainly related to the apsidal precession of Neptune. Roughly speaking, in a ν_8 resonance, the Trojan’s perihelion precesses at almost the same rate as Neptune’s perihelion does, and the difference between the longitudes of perihelion $\varpi - \varpi_8$ oscillates around a constant value with a definite amplitude. We illustrate in Fig. 8 the orbital evolution of a typical Trojan initialized in the unstable gap to show the effects of the ν_8 resonance.

As shown in Fig. 8, σ librates with a small amplitude around the Lagrange point L_5 with $\sigma \in (-65^\circ, -52^\circ)$ before 1.57×10^7 yr. Thanks to the protection of the 1:1 resonance, the evolutions of other orbital elements during this period are regular, e.g. a is nearly constant and i varies around $\sim 44^\circ$ with an amplitude of only $\sim 4^\circ$. But there is one exception, the eccentricity e is increasing during this period and it reaches $e = 0.355$ at $T = 1.57 \times 10^7$ yr. We know that the secular resonance related to the perihelion precession may drive the eccentricity up (Murray & Dermott 1999). In fact, the ν_8 secular resonance, characterized by a libration of $\varpi - \varpi_8$ as shown in the bottom panel of Fig. 8, is responsible for this eccentricity increasing.

Again, the high eccentricity, this time owing to the ν_8 resonance, reduces the Trojan’s perihelion distance, and then the object is driven out by the strong perturbations during close encounters with Uranus. We may note that after leaving the 1:1 mean motion resonance and before being scattered far away, the object temporally experiences the Kozai resonance again from 16 Myr to 20 Myr with ω oscillating, around 180° this time.

3.4 Three-body resonance

So far we discussed two mechanisms that affect the secular behavior of Trojan orbits, i.e. the Kozai resonance and the ν_8 resonance. Apart from the unstable regions due to these two mechanisms, some other chaotic subregions embedded in the dynamical map can be seen, e.g. the blue (chaotic) arc structures mentioned in Section 3.1. The possible mechanisms behind these structures are not so obvious. However, since the orbital periods of Neptune and Uranus are very close to a 2:1 commensurability (165 yr vs 84 yr), the three-body mean motion resonance (Nesorný & Morbidelli 1998) between the Trojan and them is a good guess.

For a Neptune Trojan, we expect that a three-body resonance may happen when $\dot{\lambda} + \dot{\lambda}_8 - \dot{\lambda}_7 \sim 0$. The resonant angles associated with this resonance would be any combination of the form:

$$\lambda + \lambda_8 - \lambda_7 + l\varpi + l_7\varpi_7 + l_8\varpi_8, \quad (3)$$

where l, l_7, l_8 are integers satisfying the d’Alembert rule: $l + l_7 + l_8 = -1$. Different resonances with different combinations of l, l_7 and l_8 may be responsible for the “multiplet” arc structures in the dynamical map. By testing the behavior of orbits, we find that several (but not all) Trojans initialized in the most distinct chaotic arc may be related to the l, l_7, l_8 combination of 2, -3, 0. For these orbits the angle $\lambda + \lambda_8 - \lambda_7 + 2\varpi - 3\varpi_7$ typically varies very slowly.

Table 2. The fundamental secular frequencies in the outer solar system. The period values are taken from (Nobili, Milani & Carpino 1989), from which the frequency values are computed. The periods are given in years and frequencies in $10^{-7} 2\pi/\text{yr}$. Since the resolution in frequency is $2.980 \times 10^{-8} 2\pi/\text{yr}$ in our FFT procedure, we keep two places of decimals.

	Period	Freq.		Period	Freq.
g_5	304,400.48	32.85	s_5	129,550,000.	0.08
g_6	45,883.37	217.94	s_6	49,193.46	203.28
g_7	419,858.29	23.82	s_7	433,059.42	23.09
g_8	1,926,991.9	5.19	s_8	1,871,442.70	5.34

This is an “order 5” resonance. But in fact, as we will see in next section, those arcs probably are not caused by the three-body resonance.

It is impossible and unreasonable to check all the combinations of the integers l, l_7, l_8 for all orbits inside an interesting area. To obtain a global understanding of motion on the initial plane (a_0, i_0), we turn to a frequency analysis method in next section.

4 FREQUENCY ANALYSIS

We have integrated thousands of Trojan orbits to construct the dynamical map and the filtered output from the integrations contains valuable information about the global view of the motion on the initial plane. We show in this part our frequency analysis on three basic variables in the motion: the resonant argument in the form of $\cos \sigma$ and the non-singular variables k and q , which are related to the eccentricity e and inclination i through the relations:

$$k = e \cos \varpi; \quad q = \sin i \cos \Omega. \quad (4)$$

The spectra of these variables give information about the most important rates of the resonant argument, the perihelion longitude and the nodal longitude. We denote these three proper frequencies by f_σ, g and s hereafter.

4.1 Dynamical spectrum

Typically, a power spectrum of $\cos \sigma, k$ or q is very informative but simultaneously very complicated as well. It is a complicated composition of peaks at all the forced frequencies, free frequencies, their harmonics and their combinations. Therefore a direct look at a specific power spectrum may not be very helpful. However, when we exam the continuous change of the spectrum with a parameter, some important features emerge. This continuous change of a spectrum, defined as the *dynamical spectrum*, is calculated in this paper.

We first list the fundamental frequencies (Nobili, Milani & Carpino 1989) in the outer solar system in Table 2. One frequency not listed but important in the dynamics of Neptune Trojan is the frequency of the quasi 2:1 mean motion resonance between Neptune and Uranus, $f_{2N:1U}$. The value determined from our calculation is $f_{2N:1U} = 2.3606 \times 10^{-4} 2\pi/\text{yr}$, corresponding to a period of 4236 yr.

For each orbit initialized on a horizontal or vertical

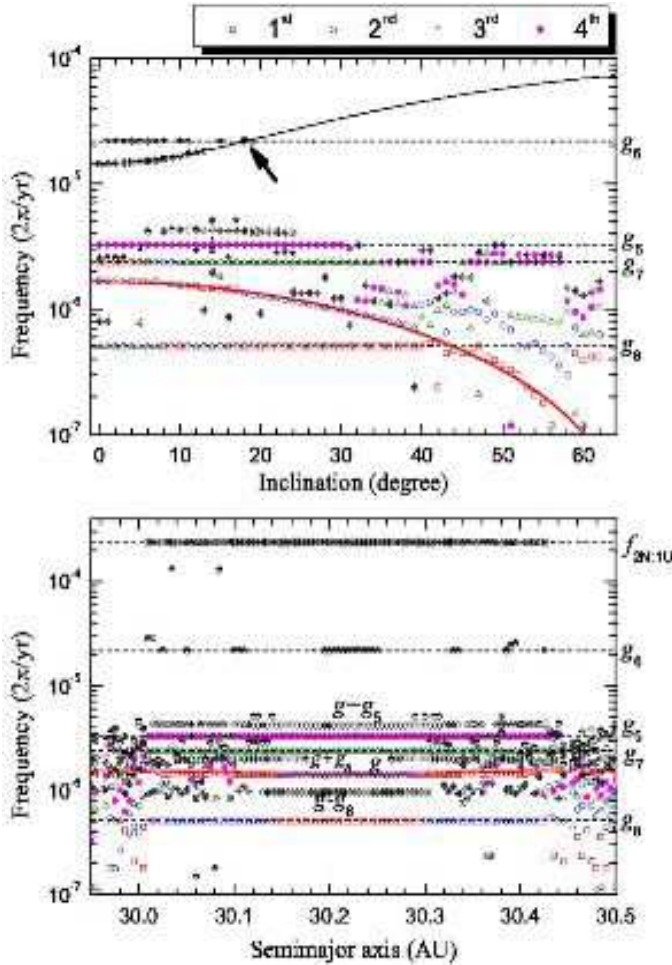


Figure 9. Dynamical spectra of the apsidal variable k . The top panel is for initial orbits on the vertical line $a_0 = 30.098$ AU on the (a_0, e_0) plane, and the bottom panel is for orbits on the horizontal line $i_0 = 15^\circ$. The frequency of the highest peak is denoted by open squares, and the frequencies of the 2nd, 3rd and 4th highest peaks are open circles, open triangles and solid circles respectively. Other frequencies are given in different type of symbols, but not labeled. The dashed lines give the values of the fundamental frequencies in the outer solar systems g_5, g_6, g_7, g_8 and the frequency of the quasi 2:1 mean motion resonance between Neptune and Uranus $f_{2N:1U}$. The thick solid curves are the numerical fit of the proper frequency of k given in Eq.(5) and the thin solid curve stands $f_{2N:1U} - 2f_\sigma$ from the numerical fit.

straight line on the (a_0, i_0) plane, the FFT is performed on the filtered output of k (or $q, \cos \sigma$) and a power spectrum is obtained. The leading terms in the spectrum are picked out for further analysis. Here by “leading terms” we mean those frequencies at which the peaks in the power spectrum are among the highest ones. We show first in Fig. 9 the variation of the leading frequencies of k along the specific lines on the (a_0, i_0) plane. The strength of the peak is not specified in number but denoted by its order in the sequence of peaks’ heights.

As shown in Fig. 9, the motion is complicated with the spectrum typically characterized by a composition of many terms at different frequencies. The peaks at the fundamental frequencies are the forced terms, and their frequencies

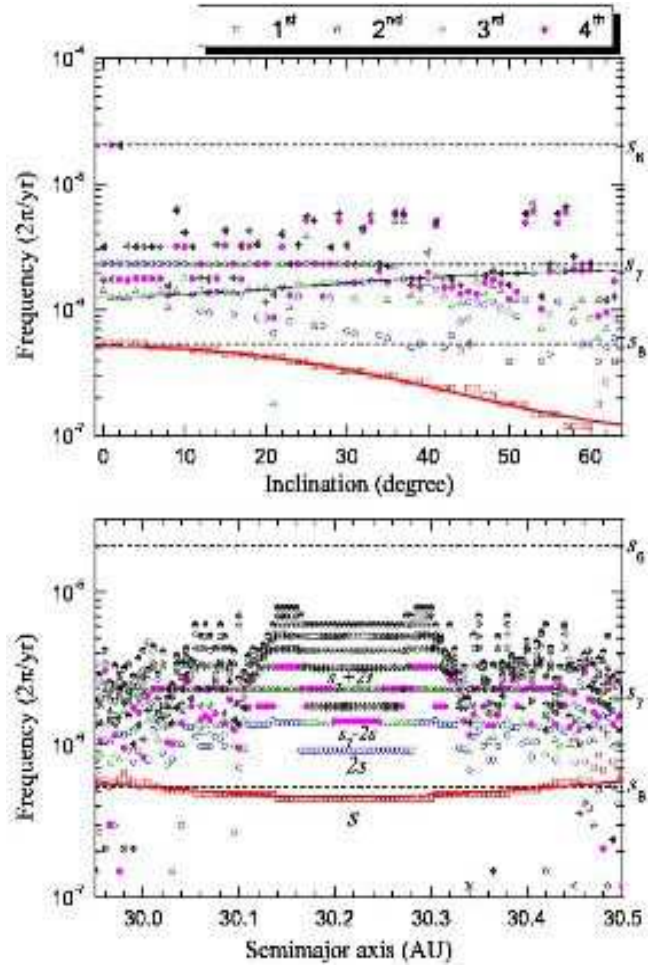


Figure 10. Dynamical spectra of the nodal variable p . The top panel is for initial orbits on the vertical line $a_0 = 30.152$ AU, and the bottom panel is for orbits on the horizontal line $i_0 = 15^\circ$. The dashed lines denote the fundamental nodal frequencies s_6, s_7 and s_8 . The frequency related to the nodal precession of Jupiter, $s_5 \sim 8 \times 10^{-9} 2\pi/\text{yr}$, is beyond the scope of this figure and can not be correctly reflected in our integration of 34 Myr. The thick solid curves stand the numerical fit of the proper frequency s in Eq.(6) and the thin solid curve in the top panel indicates the frequency of $s_7 - 2s$.

do not change with the parameters (i_0 in the top panel and a_0 in the bottom panel). The proper frequency can be easily recognized because it changes continuously with the parameter.

The proper frequency of the apsidal precession g shown in the top panel of Fig. 9 is always below g_5, g_6 and g_7 , but it meets g_8 at $i_0 \sim 43.5^\circ$ where the ν_8 secular resonance ($g = g_8$) is located. Around this resonance and also at the high inclination end, the motion is chaotic, as reflected by the discontinuity at the frequency evolution and the scattered values of frequencies.

As described above, with the help of dynamical spectrum, we can locate the position of the ν_8 secular resonance. In fact, the dynamical spectrum contains more information. For example, a frequency at low inclination can be seen approaching g_6 with increasing i_0 and meeting g_6 finally at $i_0 \sim 18^\circ$, as indicated by an arrow in the top panel. Checking

the dynamical map, we see this vertical line $a_0 = 30.098$ AU crosses the “arc structure” from $i_0 = 14^\circ$ to 20° . Around $i_0 = 18^\circ$ is a regular island surrounded by two chaotic segments at 15° and 20° . Reasonably we suspect that the arc structure arises due to this frequency crossing. A careful calculation tells us that the varying frequency seen in Fig. 9 is probably $f_{2N:1U} - 2f_\sigma$.

The proper frequency g is not necessarily the dominant frequency in the motion. As we can see in Fig. 9, the forced term associated with Uranus dominates the motion at low inclination where the highest peak (denoted by open squares) in the spectrum is the forced term at frequency of g_7 , and the forced term associated with Neptune takes over the control at higher inclination ($i_0 > 17^\circ$). Only in the range $13^\circ \leq i_0 \leq 16^\circ$, when the value of the proper frequency is far from the values of both g_7 and g_8 , the Trojan’s motion is dominated by its own proper frequency. This explains the fact that the e_{\max} in Fig. 4 reaches its maximum around $i_0 \sim 14^\circ$, because otherwise the eccentricity is suppressed by the forced oscillations.

Similar dynamical spectra for the nodal variable q are presented in Fig. 10, and a similar analysis on the dynamical spectrum can be done too. The proper frequency of the nodal precession s is far away from any fundamental frequencies except the s_8 . Although it is very close to s_8 at low inclination, the effect of secular resonance ν_{18} ($s = s_8$) seems very weak compared to the ν_8 or even some secondary resonances, as we will discuss in next subsection.

The nodal precession of the Trojan is less affected by planets. The dominant frequency in the spectrum of q is the proper frequency s , and the leading frequencies include $s, 2s, s_7, s_7 + 2s$ and $s_7 - 2s$, as shown in Fig. 10. This implies that except in the region of ν_{18} resonance, the most strong perturbation to the nodal evolution of Trojan is from Uranus.

Because of the small value ($s < 6 \times 10^{-7} 2\pi/\text{yr}$) and of the restricted resolution of FFT, the precision of s is poorer compared to g and f_σ . In this sense, a longer integration time is needed to give more accurate results about the nodal resonance of Trojan motion.

The dynamical spectrum of the resonant argument σ can also be constructed in a similar way. We do not show them here but present empirical expressions of the proper frequencies g, s, f_σ and construct a resonance map on the initial plane (a_0, i_0) .

4.2 Semi-analytical model

Knowing the values of the proper frequencies g, s and f_σ on the initial plane (a_0, i_0) , we obtain empirical expressions through numerical fitting. Set $x = a_0 - 30.219$, $y = \sin i_0$ and adopt the quadratic formula used in references (Milani 1994; Marzari, Tricarico & Scholl 2003b), the best fit of these proper frequencies from our calculations are:

$$g[10^{-6} 2\pi/\text{yr}] = 1.586 + 5.614x^2 - 2.747y^2 - 40.386x^4 + 1.192y^4 - 15.811x^2y^2 \quad (5)$$

$$s[10^{-7} 2\pi/\text{yr}] = 5.078 + 19.791x^2 - 8.218y^2 - 54.957x^4 + 4.192y^4 - 7.855x^2y^2 \quad (6)$$

$$f_\sigma[10^{-5} 2\pi/\text{yr}] = 11.349 - 17.421x^2 - 3.846y^2$$

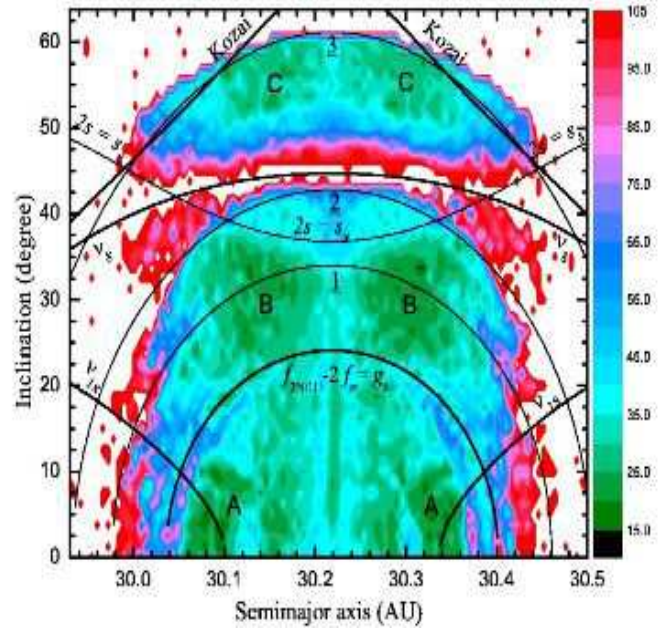


Figure 11. The main secular resonances (commensurabilities) for Trojans around the L_5 point on the (a_0, i_0) plane. The resonances are labeled along the curves. Three thin curves labeled 1, 2 and 3 represent the locations where $f_{2N:1U} - 2f_\sigma = \frac{3}{2}g_6, 2g_6$ and $3g_6$, respectively. Three most regular regions are indicated by A, B and C.

$$- 45.779x^4 + 0.230y^4 + 2.314x^2y^2 \quad (7)$$

About one thousand orbits have been used to calculate the coefficients and the precision of the fitting is guaranteed by the reduced $\chi^2 = 9.570 \times 10^{-16}, 3.799 \times 10^{-16}$ and 3.646×10^{-13} for g, s and f_σ respectively.

The value 30.219 in x is assumed to be the semimajor axis at the center of tadpole orbits around the L_5 point. The analytical formulas are symmetric with respect to this center. As we have mentioned at the end of Section 3.1, this symmetry is not “exactly” conserved actually. In addition, one should note that the analytical expressions are more accurate and reliable in the central part of the (a_0, i_0) plane where the proper frequencies are more accurately determined. Near the border between the stable and unstable region, the motion is more chaotic and the precision of the frequencies is relatively poor.

4.3 Secular resonances map

Given the analytical expressions of the proper frequencies, we can identify the main secular resonances on the initial plane (a_0, i_0) . For example, a Kozai resonance happens when $g = s$ (since $\omega = \varpi - \Omega$, $g = s$ infers $\dot{\omega} = 0$), so that the position where the Kozai resonance may arise can be calculated by solving the equation $g(x, y) - s(x, y) = 0$. In Fig. 11, we plot the major secular resonances on the initial plane. The dynamical map is plotted as the background simultaneously, providing a convenient comparison between the secular resonances and the dynamical stability.

The very good agreement, between the fine structures in dynamical map and the locations of different secular resonances, is obvious. As shown in Fig. 11, it is clear that

the unstable gap around $i_0 \sim 44^\circ$ is determined by the ν_8 resonance, the Kozai resonance can be found at high inclination, and the nodal resonance ν_{18} takes place at low inclination. On one hand, around the exact location, every resonance has a “width” in which the resonance happens and the corresponding resonant argument oscillates with a definite amplitude. On the other hand, Fig. 11 gives only the location in the phase space where the secular resonance possibly occurs. Whether a resonance actually happens depends on whether the motion is strongly influenced by other mechanisms than the resonance itself. For example, the V-shape curves in Fig. 11 indicate the position where the ν_{18} secular resonance may happen, but in fact, we only observed this resonance at low inclination with $i_0 < 1.5^\circ$. At higher inclination this resonance is hidden by other mechanisms.

From the dynamical spectrum of g in Fig. 9, we have found the equality between the frequencies of $f_{2N:1U} - 2f_\sigma$ and g_6 plays a role in forming the arc structure in the dynamical map. The curve $f_{2N:1U} - 2f_\sigma = g_6$ in Fig. 11 coincides very well with the stable arc, while curves $f_{2N:1U} - 2f_\sigma = g_6 - g$ and $f_{2N:1U} - 2f_\sigma = g_6 + g$, which are not plotted explicitly, coincide very well with the unstable arcs by the inner and outer sides of the stable one. Further calculations show that different commensurabilities between $f_{2N:1U} - 2f_\sigma$ and g_6 are most probably responsible for the multiplet arc structures, as other three curves labeled 1, 2 and 3 show in Fig. 11. Even the less regular “holes” at low inclination ($i_0 < 5^\circ$) around $a_0 = 30.13$ and 30.31 AU seem to be related with this resonance family. Our calculations show that $f_{2N:1U} - 2f_\sigma = \frac{1}{2}g_6$ and $s = g_8$ assemble in these neighbourhood. One may note that these commensurabilities are not resonances since the d’Alembert rule of invariance to rotations is not fulfilled. This is because we cannot identify the contributions of all the longitude precessions, especially those with lowest frequencies. However, the plot of these commensurabilities gives good estimate of the position of the real resonances.

As shown above, Uranus may put its influence on the stability of Neptune Trojans through the quasi 2:1 mean motion resonance. Similar effects of the quasi 5:2 resonance between Jupiter and Saturn (the Great Inequality) on the main-belt asteroids in resonance have been discussed e.g., in (Ferraz-Mello, Nesvorný & Michtchenko 1998). We argue that Saturn is also very important because its apsidal precession g_6 is deeply involved in shaping the stable region.

Surely we could not plot all the possible resonances (commensurabilities). However, we plot $2s = s_8$ in Fig. 10, because it defines the upper limit $i_0 \sim 35^\circ$ of stable region B. In a typical power spectrum of $\cos \sigma$, k or q , we can detect some less important peaks and they may evolve into some less important secular resonances. We list a few of these possible commensurabilities: $g = g_5 - g_7$, $2g = g_5$, $2g = g_7$, $2g = g_8$, $g = g_7 - 2g_8$, $2s = s_7 - 3s_8$, $3s = s_7 - 2s_8$ and $4s = s_7 - s_8$. Among them, many cross the area with $i_0 \in (12^\circ, 22^\circ)$ between the stable region A and B. They themselves or their overlapping between each other bring irregularity to the motion and therefore this area looks less stable than the neighboring region A and B.

5 CONCLUSION

Since the first Neptune Trojan was found in 2001 their number steadily increases and now we have knowledge of 6 such asteroids around the Lagrange point L_4 . It is interesting to note that two of them are on highly inclined orbits. Hence we study in this paper the orbital stability of Neptune Trojans, with special interests on the inclined orbits.

We first verified the symmetry between the L_4 and L_5 points. We found that orbits around these two points have the same stability. The only difference between them is in the value of the osculating semimajor axis of orbits at the libration center in the Trojan clouds around the L_4 and L_5 points. This difference was found due to the asymmetrical selection of initial conditions. To clarify this symmetry is important, not only because some papers argued that the L_4 and L_5 are dynamically asymmetrical to each other, but also because a specific formation history of Trojan clouds may affect the symmetry property. If future observing confirms the symmetry or asymmetry, it will put strong constraints on the formation scenario, which is tightly related to the early dynamical evolution of the outer solar system.

Using the spectral number as an indicator, we portrayed the dynamical map on the initial plane (a_0, i_0) . We found that the inclination of stable orbits could be as high as 60° . Three most stable areas were located in the dynamical map, region A with $i_0 \in (0^\circ, 12^\circ)$, B with $i_0 \in (22^\circ, 36^\circ)$ and C with $i_0 \in (51^\circ, 59^\circ)$, where the amplitude of the oscillating resonant argument is in the range of $(20^\circ - 60^\circ)$. In these regions more Trojan objects may be observed in future. The region A and B are connected to each other by an area of less regular orbits, but region C is isolated from A and B by an unstable gap at $i_0 \sim 44^\circ$. We argue that any Trojan found in region C must be a relic of the primordial Trojan cloud. At the median inclination $12^\circ - 22^\circ$, orbits are less stable but many of them can survive in the outer solar system up to 10^9 yr, and this area may host less Trojans than the stable regions. Trojans in this area would wander around for very long time before they leave the resonance.

By calculating the dynamical spectra and the proper frequencies of the resonance argument, the apsidal precession and the nodal precession, we figured out the secular resonances that generate the fine structures in the dynamical map. The upper limit of stable space in inclination about $i_0 = 60^\circ$ was found to be caused by the Kozai resonance, in which the perihelion argument librates around $\omega \sim 320^\circ$, other than the well-known values of $0^\circ (180^\circ)$ or $90^\circ (270^\circ)$. The ν_8 secular resonance was identified in the unstable gap around $i_0 \sim 44^\circ$, where the difference between the longitudes of the Trojan and Neptune $\varpi - \varpi_8$ oscillates around $\sim 270^\circ$. We also found that the nodal secular resonance ν_{18} only takes place at low inclination. By constructing the semi-analytical expressions of the proper frequencies, we analyzed the delicate structures seen in the dynamical map on the (a_0, i_0) plane. Particularly, we found that the commensurabilities between the frequencies of the quasi 2:1 mean motion resonance $f_{2N:1U}$, of the 1:1 resonant argument f_σ and of the apsidal precession of Saturn g_6 , are responsible for the multiplet arc structures in the dynamical map.

We also check how the stability of a Trojan’s orbit depends on the initial eccentricity. The preliminary results show that for most inclination values, the orbit needs a small

initial eccentricity to be stable. The largest initial eccentricity that a stable orbit may endure is $e_0 \sim 0.10, 0.12$ and 0.03 at initial inclination around $10^\circ, 35^\circ$ and 55° respectively in the three stable areas (region A, B and C). A thorough analysis on the eccentric orbits will be presented in the coming paper.

ACKNOWLEDGEMENTS

We thank Dr. X.Wan for helpful discussions. This work was supported by the Natural Science Foundation of China (No. 10403004, 10833001, 10803003), the National Basic Research Program of China (2007CB814800). RD has to thank the Austrian Science Foundation (FWF project P18930-N16) for their support. LYZ thanks University of Vienna for the financial support during his stay in Austria.

REFERENCES

- Brasser R., Heggie D., Mikkola S., 2004a, *Celest. Mech. & Dyn. Astr.*, 88, 123-152
- Brasser R., Mikkola S., Huang T.-Y., Wiegert P., Innanen K., 2004b, *MNRAS*, 347, 833
- Carpino M., Milani A., Nobili A.M., 1987, *A&A*, 181, 182
- Chambers J.E., 1999, *MNRAS*, 304, 793
- Dvorak R., Schwarz R., Süli Á., Kotoulas T., 2007, *MNRAS*, 382, 1324
- Dvorak R., Lhotka Ch., Schwarz R., 2008, *Celest. Mech. & Dyn. Astr.*, 102, 97
- Érdi B., 1988, *Celest. Mech.*, 43, 303
- Ferraz-Mello S., Nesvorný D., Michtchenko T., 1998, *Celest. Mech. Dyn. Astr.*, 69, 171
- Ferraz-Mello S., Michtchenko T.A., Beaugé C., Callegari Jr. N., 2005, in Dvorak R., Freistetter R., Kurths J., eds. *Chaos and Stability in Extrasolar Planetary Systems*, Lecture Notes in Physics, Springer, p.219
- Hanslmeier A., Dvorak R., 1984, *A&A*, 132, 203
- Holman M.J., Wisdom J., 1993, *AJ*, 105, 1987
- Kinoshita H., Nakai H., 2007, *Celest. Mech. Dyn. Astr.*, 98, 67
- Kozai Y., 1962, *AJ*, 67, 591
- Li J., Zhou L.-Y., Sun Y.-S., 2007, *A&A*, 464, 775
- Marzari F., Tricarico P., Scholl H., 2003a, *A&A*, 410, 725
- Marzari F., Tricarico P., Scholl H., 2003b, *MNRAS*, 345, 1091
- Michel P., Thomas F., 1996, *A&A*, 307, 310
- Michtchenko T., Ferraz-Mello S., 1995, *A&A*, 303, 945
- Michtchenko T., Lazzaro D., Ferraz-Mello S., Roig F., 2002, *Icarus*, 158, 343
- Michtchenko T., Beaugé C., Ferraz-Mello S., 2008, *MNRAS*, 387, 747
- Milani A., 1993, *Celest. Mech. & Dyn. Astr.*, 57, 59
- Milani A., 1994, in Milani A., Martino M., Cellino A., eds. *Proc. IAU Symp. 160, Asteroids, Comets, Meteors 1993*. Kluwer Academic Publisher, Netherlands, p.159
- Murray C.D., Dermott S.F., 1999, *Solar System Dynamics*, Cambridge Univ. Press, Cambridge
- Namouni F., 1999, *Icarus*, 137, 293
- Nesvorný D., Dones L., 2002, *Icarus*, 160, 271
- Nesvorný D., Morbidelli A., 1998, *AJ*, 116, 3029
- Nesvorný D., Thomas F., Ferraz-Mello S., Morbidelli A., 2002, *Celest. Mech. & Dyn. Astr.*, 82, 323
- Nobili A.M., Milani A., Carpino M., 1989, *A&A*, 210, 313
- Pittichova J. et al., 2003, *Minor Planet Electronic Circ.*, 2003-A55
- Sheppard S., Trujillo C., 2006, *Sci*, 313, 511
- Thomas F., Morbidelli A., 1996, *Celest. Mech. & Dyn. Astr.*, 64, 209
- Weissman P., Levison H., 1997, in Stern S., Tholen D., eds. *Pluto and Charon*. Univ. of Arizona Press, Tucson, p.559